Proceedings of the 2003 IEEE International Frequency Control Symposium and PDA Exhibition
Jointly with the 17th European Frequency and Time Forum

Atomic Clocks Based on Coherent Population Trapping: Basic Theoretical Models and Frequency Stability

J. Vanier[1,2], A. Godone[3], F. Levi[3], and S. Micalizio[3]

[1]Département de physique, Université de Montréal, , Montréal, Québec, H3C 3J7, Canada.
[2]Kernco Inc., 28 Harbor Street, Danvers, MA, 01923-0678, USA.
[3]Istituto Elettrotecnico Nazionale, Strada delle Cacce 91, 10135 Torino, Italy.

Abstract- The paper gives an overview of our present theoretical understanding of coherent population trapping in alkali metal atoms as used in the implementation of an atomic frequency standard. Two approaches are examined: The passive approach in which the microwave hyperfine resonance is detected directly on the transmitted radiation and the maser approach in which the same resonance is observed by means of stimulated emission in a microwave cavity. The theoretical analysis reviewed is supported by experimental results.

I. INTRODUCTION

Coherent Population Trapping (CPT) [1] in alkali metal atoms is a phenomenon excited by means of two coherent optical radiation fields. The fields are applied to an ensemble of atoms in resonance with the transitions between the two hyperfine levels of the $S_{1/2}$ ground state and one of the P state hyperfine levels, forming a so-called Λ system. Due to inherent physical properties, interference appears in the excitation process, coherence is created in the ground state, and the ensemble is placed in a non-absorbing state called a "dark state". The phenomenon may be used to implement an atomic frequency standard either in the passive or the active mode [2,3]. In the passive mode, the effect of the dark state, as observed in the transmitted or fluorescence radiation, is exploited. In the active mode, the oscillating magnetization created in the ensemble by the phenomenon is detected by means of stimulated emission in a microwave cavity, as in a maser [4]. In both cases, the resonance line exploited originates from the coherence created in the ensemble by the phenomenon at the ground state hyperfine frequency. This resonance line has essentially all the same properties of the ground state hyperfine resonance as is observed in the classical optical-microwave double resonance technique [5].

It is possible to interpret the phenomenon by means of a simple three-level model. The rate equations for the evolution of the energy levels populations and of the coherence created by the laser radiation fields in the ensemble may be solved exactly in the case of low alkali metal atom density [6]. The results of that analysis, however, are rather complex and are not transparent to easy interpretation. In order to interpret more easily experimental data in connection to atomic frequency standards applications, simpler theories have been developed [2,3]. In those theories, a three-level model is also used, but the rate equations are solved approximately by means of a first order analysis relative to optical coherence. The expressions obtained for the hyperfine resonance line shape, width and amplitude are transparent and easy to interpret. The results can explain most experimental data in the case of a dilute or optically thin absorbing medium. However, in the case of an optically thick ensemble, (for T>50 ^{o}C in the case of Rb, T> 40^{o}C in the case of Cs) a more elaborate approach using concepts developed in the study of the Electromagnetically Induced Transparency phenomenon, (EIT) [7], is required [8]. Furthermore, in the case when relatively intense radiation fields are used, it is found that the three-level model is not adequate. The lower manifolds of an alkali metal atom contains many energy levels and the Λ system is no longer closed as in the three level model [9]. For example, when circularly polarized radiation is used as required to observe the so-called ground state field independent 0-0 transition, atoms are optically pumped to a level not involved in the coherent population trapping phenomenon. They are transferred to, and trapped in that level: they no longer contribute to the CPT resonance phenomenon. This effect has consequences on the observed signal amplitude. This effect is also encountered in several other experimental studies related to atom cooling [10,11,12,13]. The effect is also visible on the standard absorption spectrum of laser radiation. This is discussed in the Appendix.

The present paper provides an overview of the analysis made on CPT as related to application of the phenomenon to the field of frequency standards, and evaluates these analyses in connection with their ability to explain experimental observations. In the light of those results, the paper provides an evaluation of the achievable short-term frequency stability of CPT frequency standards. The paper

gives also an overview of the various frequency shifts inherent to the CPT phenomenon, shifts that are specific to either the passive or the maser approaches, and that can affect the long-term stability of such frequency standards.

II. COHERENT POPULATION TRAPPING

Coherent population trapping in alkali metal atoms may be observed by means of the arrangement shown in Fig. 1.

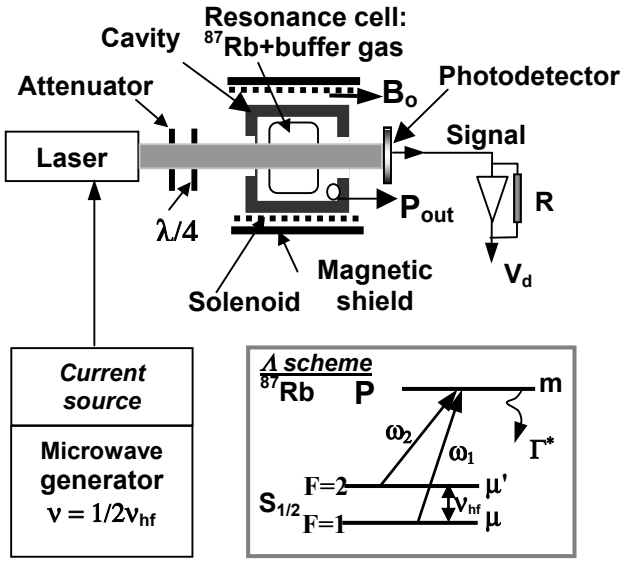

Figure 1. Experimental arrangement used to observe the CPT phenomenon in transmission. The inset illustrates the three-level model often used in the analysis of the CPT phenomenon. In the passive approach, the microwave cavity is not used

The operation of the system may be explained by means of the simple three-level model shown in the inset of Fig. 1 for the case of ^{87}Rb. In that figure, Γ^* is the decay rate of atoms from the excited state, a decay that takes place mainly through buffer gas collisions. In the ground state, relaxation takes place at the rates γ_1 and γ_2 for the populations and coherence respectively. The atomic ensemble is submitted to coherent radiation at two frequencies ω_1 and ω_2 connecting the two hyperfine levels of the ground state to a common excited state. In the case of interest for frequency standards application, the two ground state levels μ and μ' are those corresponding to $F = 2$, $m_F = 0$ and $F = 1$, $m_F = 0$. The excited state is the $P_{1/2}$ state, levels $F = 1$ or $F = 2$ separated by 812 MHz. This type of coherent excitation has been called a Λ scheme. In such a scheme, as mentioned above, interference takes place in the excitation and no transitions take place from the ground state to the excited state at exact resonance. This is reflected by an absence of fluorescence from the cell, or in other words by a "dark line" in the fluorescence spectrum. Furthermore, the system becomes transparent and, in transmission, a "bright line" is observed. These resonance lines reflect the properties of the ground state hyperfine transition of interest, as in the case of the double resonance technique used in the standard intensity optical pumping approach [5]. Observation of the dark line or of the bright line does not require a microwave cavity since they are detected directly on either the fluorescence or on the transmitted radiation. The phenomenon, however, creates also coherence in the ground state with an associated oscillating magnetization at the difference angular frequency, $\omega_1-\omega_2$, of the sidebands. This magnetization creates an oscillating magnetic field that can be detected by means of the microwave cavity illustrated in Fig.1. There is reaction of the cavity field on the atomic ensemble and stimulated emission takes place. The power radiated is detected by means of the coupling loop shown in the figure as in an active maser.

In the setup illustrated in Fig. 1, only the transmitted radiation is detected in the passive mode. The laser is a solid state diode of either the edge emitting or the VCSEL type. Its current is modulated at half the hyperfine frequency, that is ½ of 6.834 GHz in the case of ^{87}Rb. This produces, in the laser spectrum, sidebands J_n whose amplitudes are determined by Bessel's functions. The first two sidebands are separated by twice the modulated frequency and are used as the two radiation fields at ω_1 and ω_2. The $\lambda/4$ plate provides circular polarization required in the excitation process by transition selection rules. B_o is the applied magnetic induction providing an axis of quantization for the atomic ensemble. The resonance cell contains a few hundred μgrams of ^{87}Rb and a buffer gas to reduce transit time of atoms across the laser beam, and to prevent Rb relaxation on the cell walls as well as Doppler broadening of the microwave line [14, 2]. At high temperatures or high Rb densities (above 50 ^{o}C), fluorescence becomes important and creates incoherent optical pumping within the cell. This effect causes a loss of coherence in the ensemble. It must be avoided. For this reason, nitrogen, which has the property of quenching the scattered radiation, is used as a component of the buffer gas at a pressure of several hundreds of pascals. In that case, fluorescence cannot be used as a detection method of the CPT phenomenon and we shall limit the discussion to the case of transmission.

III. FREQUENCY STABILITY

In the practical implementation of frequency standards, size and frequency stability are important goals. CPT appears to offer substantial advantages relative to size over the classical intensity optical pumping technique (IOP). The matter has been discussed in some details in the case of the passive approach in which no microwave cavity is required leaving freedom in connection to the resonance cell design [15,16,17]. In the case of the maser approach, there is no oscillation threshold regarding cavity Q and radiation intensity [3]. Consequently, in that case also there is some freedom in the design of the cavity as compared to the case of the maser using intensity optical pumping, an approach

that requires a high Q cavity in order to reach threshold of oscillation [18].

In the implementation of a passive frequency standard based on the CPT phenomenon, the frequency of the microwave generator used to modulate the laser frequency is locked to the center of the resonance. This may be done by modulating the frequency of the microwave generator at a low frequency and using synchronous detection to create an error signal. If the amplitude of this modulation is of the order of ½ the resonance line width, the short term frequency stability in the limit of shot noise is given approximately by [19,20]:

$$\sigma(\tau) = \frac{K}{4\ \nu_{hf}}\sqrt{\frac{e}{I_{bg}}}\frac{1}{q}\tau^{-1/2} \qquad (1)$$

where K is a constant that depends on the type of modulation used and is of the order of 0.2, ν_{hf} is the hyperfine frequency, e is the charge of the electron, I_{bg} is the background current created by the residual transmitted radiation reaching the photodetector, τ is the averaging time and q is a quality figure defined as the ratio of the contrast C to the line width $\Delta\nu_{1/2}$:

$$q = C/\Delta\nu_{1/2} \qquad (2)$$

The contrast C is defined as the CPT signal intensity divided by the background intensity. To obtain best frequency stability, it is thus important to maximize contrast and to minimize line width. In practice, the laser spectrum is affected by amplitude and frequency fluctuations, which are additional sources of noise affecting frequency stability, and the limit of shot noise given above is not reached. For example, the amplitude noise, characterized by the relative intensity noise parameter, RIN [21], adds directly to shot noise. Eq. 1 becomes:

$$\sigma(\tau) \approx \frac{1}{\sqrt{2}}\frac{(\mathrm{RIN})^{1/2}}{4q\ \nu_{hf}}\tau^{-1/2} \qquad (3)$$

In such a case, it is also important to maximize the quality figure q. On the other hand, laser frequency fluctuations are transformed into amplitude fluctuations through various resonance mechanisms in the atomic ensemble and contribute to additional noise [22].

The CPT maser may be considered as a hybrid device emitting energy in an active way but at an angular frequency given by the difference angular frequency of the two laser sidebands, $\omega_1-\omega_2$. In that case, the frequency of the microwave generator used to modulate the laser is locked to the frequency of the maser emission line maximum by synchronous detection as in the passive case. It is thus a frequency-lock system. Considering only thermal noise, the short term frequency stability limit of the CPT maser may be written approximately as in the case of a passive maser [23]:

$$\sigma(\tau) \approx \sqrt{\frac{Fk_BT}{2P_o}}\frac{1}{Q_a}\tau^{-1/2} \qquad (4)$$

where T is the temperature of the cell-cavity arrangement, P_o is the power output of the maser, Q_a is the atomic line quality factor and F is the noise figure of the amplifier in the first stage of the receiver. Since the output frequency is the difference frequency of the correlated sidebands, laser frequency noise should not affect the CPT maser output frequency directly. However, these fluctuations may affect the maser frequency stability through the light shift that will be examined below. As in the case of the passive CPT approach it is important to minimize the line width to obtain the largest possible line Q in order to maximize frequency stability. Similarly, higher emission power improves frequency stability. However, since higher power generally leads to a greater line width, a trade off must be made.

The rest of this paper will be concentrated on the understanding of the basic physics of coherent population trapping with emphasis on the optimization of the parameters just mentioned in connection to frequency stability.

IV BASIC THEORY

The passive and active approaches for implementing a CPT frequency standard are based on common physical concepts. We will first establish these common concepts and then apply the results to each approach separately. We will review the theory for the isotope ^{87}Rb. It can be expanded easily to ^{85}Rb and ^{133}Cs by selecting the appropriate level structure and atomic constants. The ^{87}Rb lower energy level manifolds of interest for the present analysis are shown in Fig 2.

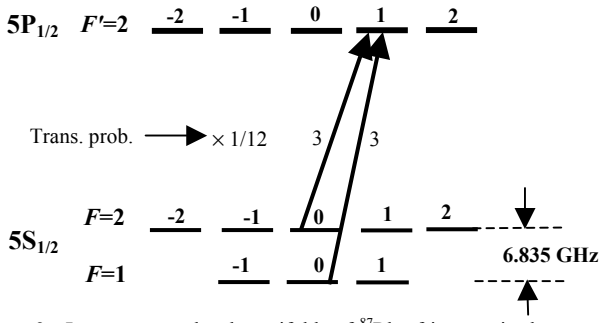

Figure 2. Lower energy level manifolds of ^{87}Rb of interest in the present analysis. The numbers attached to the transitions are transition probabilities under circular polarization (Clebsh-Gordan coefficients).

The two optical transitions (D_1 radiation at 795 nm), represented by the arrows in Fig. 2, form the Λ system mentioned earlier in the case of σ^+ polarization. These transitions connect the ground state levels F=1, $m_F = 0$, F=2,

$m_F = 0$ to a common level F' = 2, $m_F = 1$ of the excited state. They are chosen because of their higher transition probability. A similar Λ scheme for the case of the F' =1 hyperfine level could be used, but has a lower transition probability. Since the excited state hyperfine splitting is 812 MHz the optical lines are resolved up to buffer gas pressures of the order of 50 Torr, although partially overlapping. The two lower levels with $m_F = 0$ are those of interest in the implementation of a frequency standard since they are field independent in first order. Circular polarization of the radiation is required to excite the CPT phenomenon since transitions with the simultaneous conditions $\Delta F = 0$ and $\Delta m_F = 0$ are forbidden.

The four-level model

It is a general approach to isolate the three levels connected by the radiation and analyze the evolution of the ensemble of atoms as a closed system. Unfortunately, the laser radiation has a spectrum many MHz wide and all other transitions allowed under circular polarization between the $S_{1/2}$ ground state and the $P_{1/2}$ state are excited. The atoms decay from the excited state to all levels through collisions with the nitrogen molecules at the rate Γ^*. Under excitation with σ^+ polarization, level F = 2, m_F = 2, which is not connected to the excited state by the radiation, acts as a trap and atoms are lost for the Λ system of interest. This effect may be thought of as an optical pumping process filling level m_F =2 of the ground state at the expense of the other levels. The effect becomes important at high radiation intensity. In such a case it is best to represent the ensemble by means of a four-level system as shown in Fig 3, with level b representing a trap. Since relaxation in the ground state tends to reestablish equilibrium, level b may be thought of as a "leaky trap" being filled at a rate Γ* and being emptied at the rate γ_1 [24].

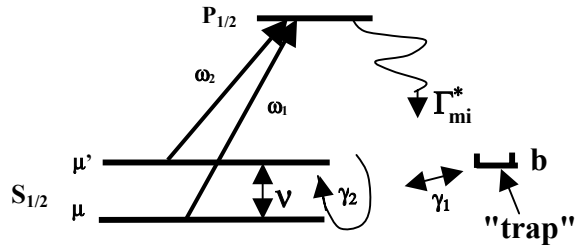

Figure 3. Four-level CPT model of ^{87}Rb used in the present analysis [24].

In frequency standard applications, the temperature of the ensemble is set around 60 °C or higher in order to obtain large signals. At that temperature the alkali metal atom density becomes large, light absorption becomes important, and the ensemble cannot be considered optically thin. It becomes inhomogeneous. In that case, in order to evaluate signal amplitude and line width, it is best to develop the analysis by means of concepts introduced in the context of the connected phenomenon called "Electromagnetically Induced Transparency" (EIT)[7].

An analysis that includes the simultaneous effect of high alkali metal atom density and optical pumping to a trapping level (open system) is rather complex. We will give an outline of this analysis in the case of the passive approach. In the case of the CPT maser the analysis in the general case of an optically opaque open system has not been done yet. We will outline the expected results in the case of a dilute ensemble.

Rate equations

The electric component of the laser radiation fields, corresponding to the sidebands J_{1+} and J_{1-}, is assumed of the form:

$$E_n(\omega_n,\ z,\ t) = E_{on}(z,\ t)\, e_\lambda \cos(\omega_n t + k \bullet r) \qquad (5)$$
$$(n = 1, 2)$$

where e_λ is the polarization vector, k is the wave vector, z is the distance traveled by the wave as measured from the cell entrance. This coherent radiation field interacts with the ensemble and creates a polarization P_n. E_n and P_n are connected by the relation [5].

$$\frac{\partial^2 E_n}{\partial z^2} - \frac{1}{c^2}\frac{\partial^2 E_n}{\partial t^2} = \mu_0 \frac{\partial^2 P_n}{\partial t^2} \qquad (6)$$

where c is the speed of light and μ_0 the permeability of free space. On the other hand, the polarization is given by:

$$P = n\ \mathrm{Tr}(\rho P_{op}) \qquad (7)$$

where n is the Rb density, ρ is the density matrix of the ^{87}Rb atom ensemble and P_{op} is the equivalent quantum mechanical operator of the classical electrical polarization. In that expression "Tr", means the trace of the product of the two matrices ρ and P_{op}. After some algebra and assuming a stationary state in which the parameters vary slowly with time relative to the optical decay times involved in the system we obtain:

$$\frac{\partial E_n}{\partial z} = \left(\frac{n\ \omega_n d_{ij}}{c\varepsilon_o}\right) \mathrm{Im}\delta_{ij}(z) \qquad (8)$$

where ω_n the laser sideband angular frequency, ε_o the permittivity of free space, d_{ij} the Rb atom electric dipole moment for transition i to j. d_{ij} contains the appropriate information on the transition probability of the transitions involved.

$\mathrm{Im}\delta_{ij}$ is the imaginary part of the optical coherence (density matrix) created in the system by the laser radiation. It is obtained through an analysis of the rate equations of the

density matrix representing the ensemble as obtained from Liouville's equation,

$$\frac{\partial \rho}{\partial t} = \frac{1}{i\hbar}[H, \rho] \tag{9}$$

where H is the interaction Hamiltonian. We introduce the Rabi angular frequency defined as

$$\omega_{R1} = (E_1/\ ) \langle \mu | e\ \boldsymbol{r} \bullet \mathbf{e}_\lambda | m \rangle \tag{10a}$$
$$\omega_{R2} = (E_2/\ ) \langle \mu' | e\ \boldsymbol{r} \bullet \mathbf{e}_\lambda | m \rangle \tag{10b}$$

for each radiation field E_1 and E_2. In the case of the maser, the atoms interact with the microwave magnetic field B_z in the cavity. We assume that the field is in the z direction parallel to the dc field, with frequency $\omega_{\mu w}$ and phase ϕ.

$$\boldsymbol{B}_{\mu w}(z, t) = \boldsymbol{z}\, B_z(z) \sin(\omega_{\mu w} t + \phi) \tag{11}$$

The associated Rabi angular frequency is defined as

$$b(z) = \mu_z B_z(z)/ \tag{12}$$

We expand Eq. (8) in terms of the various matrix elements along the lines of the procedures already established in this context [3,8,25]. We assume a solution of the resulting rate equations of the form:

$$\rho_{\mu\mu'}(z,t) = \delta_{\mu\mu'}(z,t) e^{i[(\omega_1 - \omega_2)t - (k_1 - k_2)z]} \tag{13}$$

$$\rho_{\mu m}(z,t) = \delta_{\mu m}(z,t) e^{i[\omega_1 t - k_1 z]} \tag{14}$$

$$\rho_{\mu' m}(z,t) = \delta_{\mu' m}(z,t) e^{i[\omega_2 t - k_2 z]} \tag{15}$$

We also assume homogeneous broadening of the optical line due to buffer gas collisions, and Dicke narrowing at the hyperfine frequency of the ground state [14]. In stationary state, we obtain the set of equations that applies to the four level system shown in Fig. 3:

$$\Gamma^* \rho_{mm} = -\omega_{R1}\, \mathrm{Im}\, \delta_{\mu m} - \omega_{R2}\, \mathrm{Im}\, \delta_{\mu' m} \tag{16}$$

$$\gamma_1 (\rho_{\mu'\mu'} - \rho_{\mu\mu}) = -2\mathrm{Im} i b e^{-i\phi} \delta_{\mu\mu'} + \omega_{R2} \mathrm{Im} \delta_{\mu' m} - \omega_{R1} \mathrm{Im} \delta_{\mu m} + (\Gamma^*_{m\mu'} - \Gamma^*_{m\mu}) \rho_{mm} \tag{17}$$

$$[\gamma_2 + i(\omega_{12} - \omega_{\mu'\mu})] \delta_{\mu\mu'} = i(b/2) e^{i\phi} \Delta + i(\omega_{R1}/2) \delta_{m\mu'} - i(\omega_{R2}/2) \delta_{\mu m} \tag{18}$$

$$(\Gamma^*/2 + i(\omega_1 - \omega_{m\mu})) \delta_{\mu m} = i(\omega_{R1}/2)(\rho_{mm} - \rho_{\mu\mu}) + (b/2) e^{i\phi} \delta_{\mu' m} - i(\omega_{R2}/2) \delta_{\mu\mu'} \tag{19}$$

$$(\Gamma^*/2 + i(\omega_2 - \omega_{m\mu'})) \delta_{\mu' m} = i(\omega_{R2}/2)(\rho_{mm} - \rho_{\mu'\mu'}) + (b/2) e^{i\phi} \delta_{\mu m} - i(\omega_{R1}/2) \delta_{\mu'\mu} \tag{20}$$

$$\gamma_1 \rho_{bb} = (1/3)\gamma_1 - \Gamma^*_{mb} \rho_{mm} \tag{21}$$

where

$$\omega_{12} = \omega_1 - \omega_2 \tag{22}$$

$$\rho_{mm} + \rho_{\mu'\mu'} + \rho_{\mu\mu} + \rho_{bb} = 1 \tag{23}$$

and

$$\Gamma^* = \Gamma^*_{m\mu} + \Gamma^*_{m\mu\mu} + \Gamma^*_{mb} \tag{24}$$

We note that the population ρ_{mm} of the excited state is always small (10^{-6}) relative to that of the ground levels and we have assumed that in equilibrium in the absence of radiation, the ground state levels have equal populations:

$$\rho_{\mu'\mu'}(\mathrm{eq.}) = \rho_{\mu\mu}(\mathrm{eq.}) = \rho_{bb}(\mathrm{eq.}) = \frac{1}{3} \tag{25}$$

These equations are similar to those given in [3] except for the addition of (21) for level b and the distribution of populations in three ground state levels instead of two. This addition has a direct effect on the amplitude of the ground state coherence since at high pumping rates, atoms tend to accumulate in level b.

The passive approach.

In that case the setup does not include a microwave cavity and b is set equal to zero in (16) to (21). The parameter measured is the intensity of the radiation at the exit of the cell and can be calculated by means of (8). To simplify the calculation, we assume that the two J_1 sidebands have equal amplitudes, which implies that

$$\omega_{R1} = \omega_{R2} = \omega_R\ . \tag{26}$$

In the presence of quenching by the buffer gas, we assume that the decay rates from the excited state to all levels of the ground state are equal:

$$\Gamma_{m\mu}{}^* = \Gamma_{m\mu'}{}^* = \Gamma_{mb}{}^* = \Gamma^*/3, \tag{27}$$

Using definitions (10a) and (10b), (8) may be written in terms of the Rabi frequency as

$$\frac{\partial \omega_R}{\partial z} = \alpha\, \mathrm{Im}\, \delta_{\mu m} \tag{28}$$

where the absorption coefficient α is defined as:

$$\alpha = \left(\frac{\omega}{c \varepsilon_o \hbar} d^2_{\mu m} \right) n \tag{29}$$

At the density of operation in the experiments reported below, α is of the order of 2 to 10×10^{11} $m^{-1}s^{-1}$. The optical coherence $\delta_{\mu m}$ is obtained as a solution of the stationary state equations (19) and (20):

$$\delta_{\mu m} = i\frac{(1/2)\omega_R}{(1/2)\Gamma^* + i\Omega_{op}}(\rho_{mm} - \rho_{\mu\mu} - \delta_{\mu\mu'}) \qquad (30)$$

where Ω_{op} stands for ω_l - $\omega_{\mu m}$. A similar equation is obtained for $\delta_{\mu' m}$. Due to the symmetry introduced by the modulation we have ω_l - $\omega_{\mu m}$ = ω_2 - $\omega_{\mu' m}$. We assume $\rho_{\mu\mu}$ = $\rho_{\mu'\mu'}$ because of the symmetry of the excitation, and after some algebra we obtain:

$$\rho_{bb} = \frac{1}{3} + \frac{(4/9)(\Gamma_p/\gamma_1)}{1+(2/3)(\Gamma_p/\gamma_1)} \qquad (31)$$

$$\mathrm{Im}\,\delta_{\mu m} = -\frac{\omega_R}{\Gamma^*}\left(\frac{1}{3} - \frac{(2/9)(\Gamma_p/\gamma_1)}{1+(2/3)(\Gamma_p/\gamma_1)} + \delta^r_{\mu\mu'}\right) \qquad (32)$$

where $\delta^r_{\mu\mu'}$ is the real part of the ground state coherence $\delta_{\mu\mu'}$ given by:

$$\delta_{\mu\mu'} = \frac{-(2/3)\Gamma_p(\gamma_2+2\Gamma_p) + (4/9)\dfrac{\Gamma_p^2(\gamma_2+2\Gamma_p)}{\gamma_1(1+2\Gamma_p/3\gamma_1)}}{(\gamma_2+2\Gamma_p)^2 + (\omega_{12}-\omega_{\mu'\mu})^2} + i\frac{\left((2/3)\Gamma_p - (4/9)\dfrac{\Gamma_p^2}{\gamma_1(1+2\Gamma_p/3\gamma_1)}\right)(\omega_{12}-\omega_{\mu'\mu})}{(\gamma_2+2\Gamma_p)^2 + (\omega_{12}-\omega_{\mu'\mu})^2} \qquad (33)$$

In these equations, to simplify writing, we have defined the pumping rate Γ_p, function of distance into the cell, as:

$$\Gamma_p(z) = \frac{\omega_R^2(z)}{2\Gamma^*} \qquad (34)$$

In order to obtain the value of the radiation intensity at the exit of the cell, (28) needs to be solved with $\mathrm{Im}\delta_{\mu m}$ and $\delta^r_{\mu\mu'}$ given by (32) and (33). Unfortunately, due to the complexity of the right hand side, (28) cannot be solved analytically and a numerical approach is required in which $\omega_R^2(z)$ is evaluated at the exit of the cell, that is z =L.

The line width

In view of the form of $\delta_{\mu\mu'}$, the resonance line shape is assumed to be Lorentzian with a width given by

$$\Delta\nu_{1/2} = (1/\pi)(\gamma_2 + \omega_R^2(z=L)/\Gamma^*) \qquad (35)$$

where γ_2 is the relaxation rate in the absence of laser radiation or ω_R=0. γ_2 includes several mechanisms such as relaxation by diffusion to the cell walls, relaxation by collision with the buffer gas molecules, and spin exchange interaction between Rb atoms [5,16].

Experimental results

A typical experimental result for line width and contrast is shown in Fig. 4. These results are for a cell, 23 mm long, 35 mm in diameter, filled with 11 Torr of a mixture of Ar/N_2 in the pressure ratio of ~1.4, at a temperature of 75 ^oC. An edge emitting laser diode was used and the radiation beam was about 8 mm in diameter. As is readily observed the line width is directly proportional to laser intensity. It provides a means of evaluating directly the value of the Rabi angular frequency by means of (35). On the other hand, in the present situation, the contrast appears to increase to a maximum value of the order of 5% at an intensity of about 3 V at the detector (30 μW) and decreases above that value. These measurements were repeated at four different temperatures and the results for the contrast are shown in Fig. 5. As expected, at high temperatures the density increases and the signal contrast gets larger. However, the ensemble becomes more opaque and the maximum contrast is reached at higher light intensity.

The line width was also measured at these temperatures as a function of light intensity. All measurement showed a linear dependence of $\Delta\nu_{1/2}$ versus V_d according to the relation

$$\Delta\nu_{1/2} = \Delta\nu_{1/2}(V_d = 0) + A\,V_d\,, \qquad (36)$$

where A is the slope of the dependence of the line width on light intensity represented as V_d.

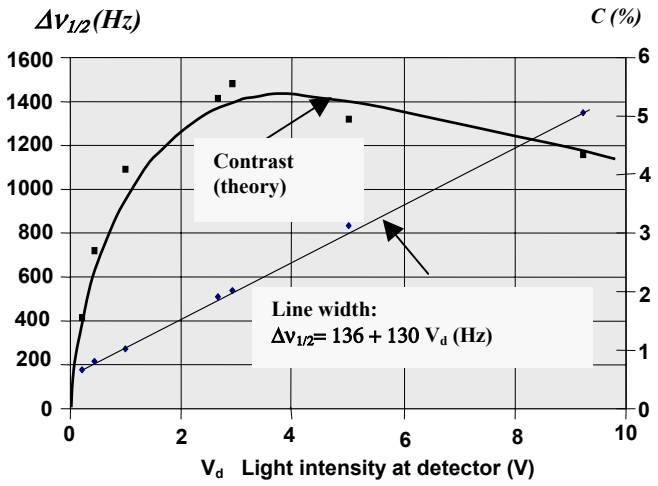

Figure 4. CPT line width (diamonds) and contrast C (squares) observed in a typical experimental situation in ^{87}Rb at 75 ^oC. The curve identified as "theory" is obtained from calculation explained in the text. The light intensity is identified as V_d. 1 volt corresponds to an incident radiation intensity of 10 μW [20].

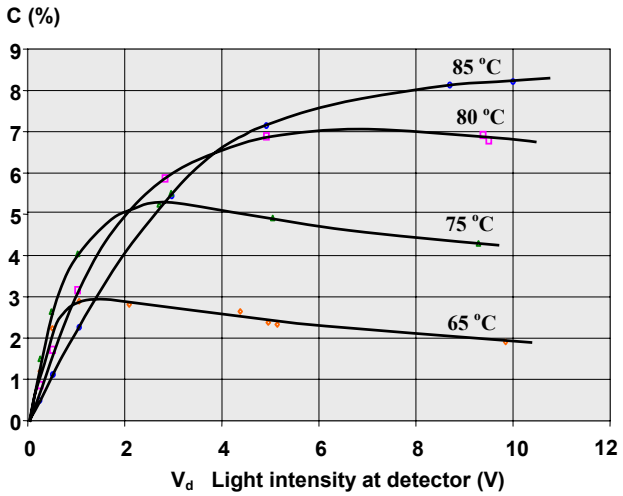

Figure 5. Contrast of CPT hyperfine resonance line measured at four temperatures as a function of light intensity [24].

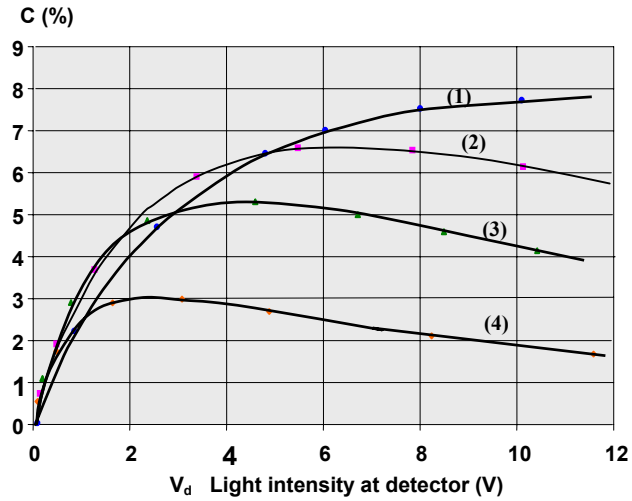

Figure 6. Theoretical contrast of the CPT hyperfine resonance in transmission as calculated by means of. (28), (32) and (33). The curves are identified as (1): $\alpha = 9.4 \times 10^{11}$ m^{-1} s^{-1}; (2) $\alpha = 6.6 \times 10^{11}$ m^{-1} s^{-1}; (3): $\alpha = 4.5 \times 10^{11}$ m^{-1} s^{-1}; (4): $\alpha = 2.1 \times 10^{11}$ m^{-1} s^{-1}. These values are proportional to the temperatures identified in Fig. 5 [24].

In all figures, the voltage developed at the detector corresponds approximately to a sensitivity of 0.1 V per microwatt.

Comparison with theory

The results relative to line width were used for calibrating the system in terms of the Rabi angular frequency vs. the detector voltage by means of (35) and (36). With these results it was then possible to evaluate numerically the expected contrast, taking into account all the sidebands contributing to the background radiation. The value of the excited state decay rate was evaluated from measurements of the optical line widths in excess of the Doppler broadening. The results of this calculation using (28), (32) and (33) are shown in Fig. 6. In the calculation, the absorption coefficient α was adjusted to a value such as to approximate the contrast observed at 75 °C. This is shown in Fig. 4. For the other temperatures the value of α, normalized to its value at 75 °C, was calculated by means of (29), *n* being determined by the temperature.

As is readily observed, the results of this calculation are in good qualitative agreement with the results obtained experimentally. The shape of the four contrast curves and the position of the maxima, calculated for the values of α obtained by the method outlined above, reproduce rather well the general behavior of the experimental results shown in Fig. 5. It was also found that the calculated line width for the four values of α used were always linear with light intensity. All line width theoretical results were within 1 % of the experimental data.

It may be mentioned that the question of CPT signal amplitude as function of temperature and light intensity has been addressed previously [26]. However, the model used in that article is based on the assumption that the amplitude of the CPT signal is due essentially to classical optical absorption by the ensemble (Beer's law), a model that is not appropriate [8]. Furthermore, in the experiments reported in that article, neon was used as buffer gas. Consequently, the experimental results were most probably affected by relaxation introduced by the fluorescence radiation as well as radiation trapping since neon does not quench fluorescence.

Maser approach: Power output

In the case of the CPT maser the analysis is more complex in view of the interaction of the atoms with the microwave field in the cavity. The analysis must take into account the phase relationship ϕ between the microwave field and the oscillating magnetization. Furthermore, the phase of the optical fields is coupled to the hyperfine coherence. An analysis taking into account the interrelation between these phases has been developed in the case of a closed three-level system. The analysis of the CPT maser characteristics including optical pumping in an open system is relatively more complex and has not been developed yet in the general case where the ensemble is optically opaque.

In order to obtain some insight into the effects of this phenomenon we will assume that the ensemble is homogeneous. The analysis will thus be valid for low temperatures. At high temperatures, however, the fact that the cell becomes optically opaque should alter those results since the atomic ensemble becomes inhomogeneous. It is expected nevertheless that the general conclusions reached in the homogeneous model regarding power against pumping rate should be approximately valid.

Homogeneous model

An analysis, as is done in standard maser theory, leads to the following relation between power output and the hyperfine coherence created in the system by the optical coherent fields [3,27]:

$$P_a = \frac{1}{2}\hbar\omega_{\mu'\mu} N_a \frac{|b_c|^2}{k} \qquad (37)$$

where b_c is the complex microwave Rabi frequency, N_a is the number of atoms interacting with the laser radiation, k is the so-called gain factor defined as:

$$k = \frac{N_a Q_a \eta' \mu_B^2 \mu_o}{\hbar V_a} \qquad (38)$$

where Q_a is the atomic line Q, η' is the filling factor, μ_B is the Bohr magneton, and μ_o is the permeability of free space. This factor k is the number of microwave photons emitted per second by the atoms. Algebraic manipulations of the set of equations (16) to (21) provide relations for phase, coherence and population difference $\Delta = \rho_{\mu'\mu'} - \rho_{\mu\mu}$. Using the equation that couples the field and the oscillating magnetization, we obtain [28]:

$$\delta_{\mu\mu'}^{r\ 3} \frac{4k^2}{\gamma_1 + 2\Gamma_p} + \delta_{\mu\mu'}^{r}(\gamma_2 + 2\Gamma_p) = -\Gamma_p \frac{2/3}{1 + 2\Gamma_p/\gamma_1} \qquad (39)$$

$$\Delta = -\frac{4k}{\gamma_1 + 2\Gamma_p} \delta_{\mu\mu'}^{r\ 2} \qquad (40)$$

$$|b|^2 = 4k^2 |\delta_{\mu\mu'}|^2 \qquad (41)$$

The phase relationship provides an equation for the cavity pulling effect as

$$\Delta\omega = \frac{Q_L}{Q_a} \Delta\omega_c (S - 1) \qquad (42)$$

where S is the ratio of the total power broadened line width to the line width caused only by relaxation and optical pumping. It is a measure of the microwave power broadening. We note that the populations of the two ground state levels that are part of the Λ system are not equal and that Δ is no longer equal to zero. This effect introduces a frequency shift similar to the light shift that is caused by asymmetry in the sidebands.

The value of $\delta_{\mu\mu'}$ is obtained from a numerical solution of (39), and the power output is obtained from (37) and (41). The results of this calculation are given Fig. 7 for three values of the gain factor k.

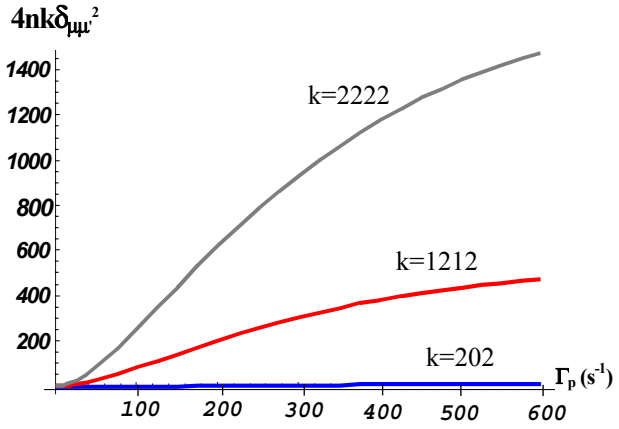

Figure 7. CPT maser calculated emitted power versus pumping rate for three values of the gain factor in the homogeneous model including a trapping level.

Inhomogeneous model

In the case of an optically thick ensemble, the amplitude of the various parameters varies along the length of the cell and the set of equations (16) to (21) are valid only locally, that is for a thin slice of the medium. Furthermore, the phases of the laser sidebands when taken into account are coupled to the microwave field and vary along the length of the cell. The problem was solved in the case of a closed three-level system by means of a numerical integration over the cell length of the Rabi frequency *b*, which is function of distance and sidebands phase [23].

It is found in particular that the calculated maser power is a function of the ratio of cell length to wavelength (microwave). In fact, for very low densities, and a cell whose length *L* is equal to $\lambda_{\mu w}$, the power output is equal to zero. This effect results from the fact that the elementary magnetizations in each slice emit with their own phase. However, at high densities, the system is not homogeneous and the phase cancellation from one part of the cavity to the other is not exact: the part of the cell at the entrance of the cavity contributes more than the part at the exit of the cavity since radiation is strongly absorbed. Nevertheless, the power calculated decreases for cell lengths slightly larger than ~λ/2.

Experimental results for the maser power output versus the transversal pumping rate are shown in Fig. 8 [23]. The curves refer to three different temperatures as indicated. A difference between the experimental behavior and the theory can be observed. In fact, theory predicts a power output proportional to the square of the density of the emitting ensemble. This is a basic consequence of the stimulated emission process that takes place in a cavity: the field created by the atoms reacts back on the same atoms and causes stimulated emission. This is not observed experimentally as it appears that the measured power

increases almost linearly with density. The difference may be due to several causes. In particular there may be some residual radiation trapping in the ensemble due to incomplete quenching, although the effect would be more important at high light intensity. The difference may also originate from the fact that the atomic ensemble is not homogeneous. At high densities the laser radiation is largely absorbed at the entrance of the cell. The consequence of this effect is to reduce the size of the contribution of successive slices to the power output. A more elaborate analysis, including at the same time the inhomogeneous model and optical pumping to a trap may elucidate this apparent difficulty.

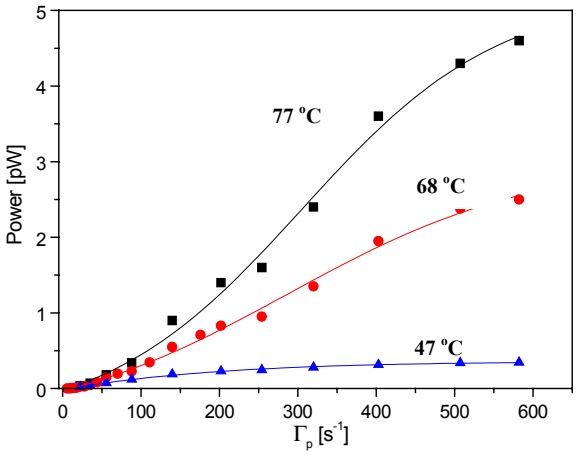

Figure 8. CPT maser power output at the receiver for three different temperatures as a function of pumping intensity [25].

V FREQUENCY STABILITY AND SHIFTS

The possible frequency stability of the passive and the maser CPT frequency standard can be evaluated from the analysis just made.

Passive frequency standard

The frequency stability is given by (1) in the limit of shot noise. The quality figure q is obtained from the contrast and the line width as calculated above. For a temperature of the order of 65 to 70 °C a q figure of the order of 1.5×10^{-4} for a background intensity I_{bg} 10×10^{-6} A is observed. The resulting expected frequency stability is of the order $7 \times 10^{-14}\tau^{-1/2}$.

Unfortunately such frequency stability is not observed in the laboratory. A frequency stability of the order of $3 - 5 \times 10^{-11}\tau^{-1/2}$ has been common observation, 2 orders of magnitude lower than that expected from the limit of shot noise [16]. It should also be mentioned that this behavior is also reported in the case of the classical passive IOP frequency standard using a solid state diode laser as the optical pumping source [29].

It is believed that this behavior is due to the inherent AM and FM noise imbedded in the laser radiation. The AM noise appears directly at the photodetector as intensity noise and adds directly to shot noise. This noise contributes to the order of a few parts in 10^{-13} to the frequency instability and of course depends on the relative intensity noise (RIN) of the laser used.. On the other hand, it is believed that the laser FM noise is converted into AM fluctuations by the nonlinear optical resonance absorption within the ensemble [22]. It adds directly also to shot noise at the detector. Experiments have been made in order to compensate this effect by either reducing the spectral width of the laser spectrum or by direct compensation by means of a clone resonance cell in the IOP approach [30]. Relative success was obtained in that last case and although the technique is somewhat complex it appears to provide an appropriate direction for reducing the effect.

Maser frequency standard.

The situation is somewhat simpler in the case of the CPT maser. The parameters in Eq.4 are directly evaluated from the previous analysis. At ~65 °C the power delivered by the atoms to the cavity is approximately 15×10^{-12} watt. The line width is of the order of 275 Hz providing a line Q_a of 2.5×10^7. With a receiver noise figure of 3 and a cavity coupling of unity, the short-term frequency stability of the maser is evaluated to be $\sim 1.5 \times 10^{-12}\,\tau^{-1/2}$. An experimental setup in which a crystal oscillator was locked to the maser power output maximum gave a stability of $4.8 \times 10^{-12}\tau^{-1/2}$.

The above evaluation does not take into account other sources of noise such as that introduced at twice the modulation frequency used in the frequency-lock loop (Dick effect), which for the crystal oscillator used in that experiment was evaluated to be of the order of $2.5 \times 10^{-12}\tau^{-1/2}$. It would be possible to improve frequency stability through the use of a more stable crystal oscillator and the use of a lower noise figure receiver. In that case for a noise figure F of 1.2 and a line Q_a of 3.7×10^7, a condition possible through a proper choice of experimental conditions, an ultimate frequency stability of $7 \times 10^{-13}\,\tau^{-1/2}$ appears possible in the short term region of averaging times. This maser performance is compared to other atomic frequency standards in Fig. 9.

Stationary frequency shifts.

The main perturbation affecting the frequency of both the passive CPT frequency standard and the CPT maser are the applied magnetic field, the buffer gas shift and the light shift. Instability in these shifts may affect frequency stability in the medium and long-term region of averaging times.

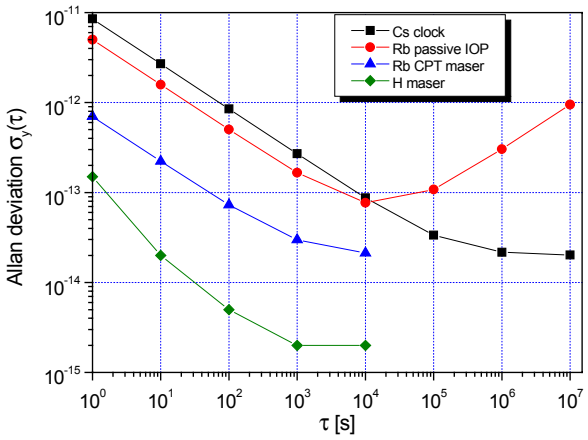

Figure 9. Frequency stability of an experimental CPT Rb maser compared to other atomic frequency standards commonly referred to in the literature [23].

Magnetic field: A magnetic field is required to provide an axis of quantization to the system and a reference axis for laser radiation polarization. The magnetic field removes Zeeman degeneracy in the ground state. The $m_F = 0$ sublevels are shifted quadratically causing a shift of the hyperfine frequency according to the equation:

$$\Delta\nu_B(^{87}\mathrm{Rb}) = 575.14 \times 10^8 B_o^2 \text{ Hz} \qquad (43)$$

where B_o is the magnetic induction in tesla. This field is generally created by means of a solenoid inside a magnetic shield. It is of the order of a few tens of μT. The current driving this field and the shielding factor must be compatible with the frequency stability desired.

Buffer gas shift and temperature coefficient: The buffer gas causes a frequency shift. This shift is proportional to the buffer gas density or, in a sealed cell, to its pressure *P*. Furthermore, this shift is temperature sensitive. The hyperfine frequency is shifted by [5]:

$$\Delta\nu = P(\beta + \delta\,\Delta T + \gamma\,\Delta T^2) \qquad (44)$$

where β is the pressure coefficient, δ is the linear temperature coefficient and γ is the quadratic temperature coefficient. Two buffer gases widely used are nitrogen and argon that have opposite pressure and temperature coefficients. In that case the coefficients of (44) are combinations of the individual buffer gas coefficients. When mixed in the ratio of pressures $R=P_{Ar}/P_{N2}$ ~1.5 the linear temperature coefficient is nearly cancelled and the residual temperature coefficient is generally less than 10^{-10} per ^oC. However, due to the presence of the quadratic term in (44), the residual coefficient is function of the temperature of operation and can be minimized by appropriate adjustment of the ratio R for the desired temperature [31].

The light shift: In the case of the CPT maser, it is found that the light shift is given by [28] :

$$\Delta\omega_{LS} = -\frac{(1-\beta^2)\,\omega_{R1}^2}{4}\left\{\frac{\Delta_0}{\left(\Gamma^*/2\right)^2 + \Delta_0^2}\right\} \qquad (46)$$

where β is the ratio of the two sidebands amplitude, J_{1+} and J_{1-}, used to create the CPT phenomenon, and Δ_o is the detuning of the laser average frequency from resonance. This is a linear light shift directly associated with the detuning of each laser radiation field from their respective transition. If the radiation fields have the same intensity, then β=1, both levels are displaced equally and there is no light shift.

In the case of the passive standard approach, a computer calculation shows that the resonance line is distorted when both β and Δ_o are different from zero. However, the minimum of the dark line does not shift with those parameters [32].

In both cases, however, maser and passive CPT approaches, there is also present a light shift caused by each laser radiation field interacting with the other optical transition. Furthermore, the interaction of the residual carrier and of all the sidebands with the two transitions concerned must be included in the calculation. A detailed calculation based on the three-level model, shows that the light shift is given by the following expression [33]:

$$\frac{\Delta\omega_{LS}}{\omega_{\mu\mu'}} = \left(\frac{\omega_{RL}}{\omega_{\mu\mu'}}\right)^2\left\{\Theta(m)+\xi(m)\left(\frac{\Delta_o}{\omega_{\mu\mu'}}\right)^2\right\} \qquad (47)$$

where

$$\Theta(m) = J_o^2(m) + (1/2)J_{p/2}^2(m) - 2\sum_{n=1\neq p/2}^{\infty} J_n^2(m)\left(\frac{p^2}{(2n)^2-p^2}\right) \qquad (48)$$

$$\xi(m) = 4J_o^2(m) - 8\sum_{n=1\neq p/2}^{\infty} J_n^2(m)\frac{12n^2+p^2}{\left((2n)^2-p^2\right)^3}p^4 \qquad (49)$$

In these expressions the J_n's are Bessel functions giving the amplitude of the sidebands and p is the ratio of the hyperfine frequency to the laser modulation frequency. When the J_1's are used to create the CPT phenomenon, p = 2. These parameters are plotted in Fig. 10.

It is readily seen that the power light shift (Θ) is minimized for a modulation index m = 2.4 [33,34]. The quadratic light

shift is not as important since the laser can be tuned such as to make it negligible.

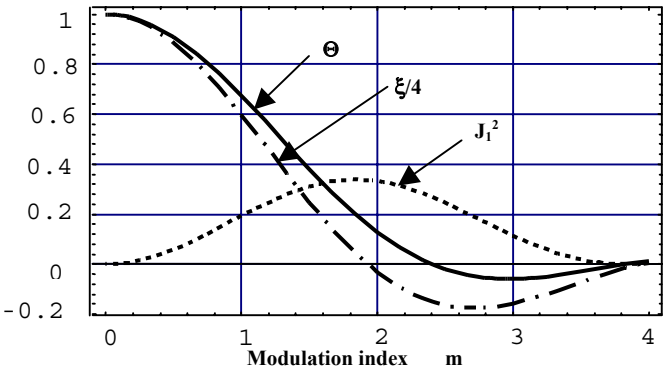

Figure 10. Variation of the light shift coefficients with modulation index in the case the first sidebands J_{1+} and J_{1-} are used to excite the CPT phenomenon [33].

Experimental results relative to these shifts are shown in Figs. 11 and 12 in the case of the CPT maser. As is clearly observed in Fig. 11, the power light shift is close to zero for a modulation index m=2.4. However there is a small dependence on temperature. This effect is due to the propagation shift to be discussed below. The quadratic light shift is clearly observed in Fig. 12 at low temperature where the maser gain is low. In the case of high pumping rates or high gain, the microwave shift becomes evident acting itself as a light shift. It is noted that these two shifts, propagation and microwave shifts, are an inherent characteristics of the CPT maser and are not present in the case of the passive approach.

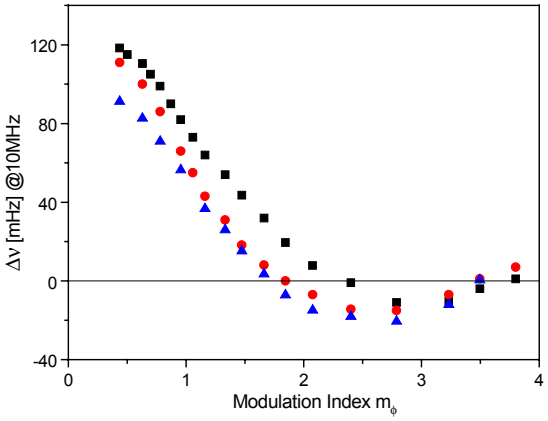

Figure 11. Power light shift as observed in a CPT Rb maser. Squares: 45 °C; filled circles: 68 °C; diamonds: 75 °C [23].

The power light shift has also been measured in the case of the passive approach and a result similar to that shown in Fig. 11 has been reported [15].

There are cases when it may be desirable to use the carrier J_o and one of the first sidebands J_1 to excite the CPT phenomenon. In that case, the light shift is given by an expression similar to (47). The power light shift is the same and is equal to zero for a modulation index of 2.4. However, the expression contains a term linear in frequency detuning Δ_o that is zero for a modulation index of 1.4. Furthermore the quadratic light shift coefficient is always positive. Consequently this approach may not be as interesting as the previous one for implementing a frequency standard since both power and linear coefficients cannot be made equal to zero at the same modulation index.

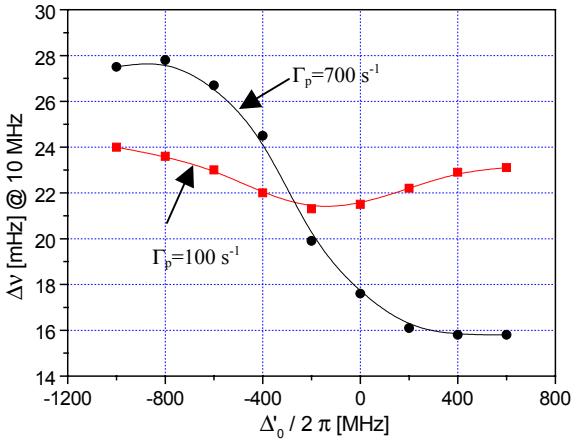

Figure 12. Quadratic light shift as observed in a CPT Rb maser [23].

Shifts particular to the CPT maser: The interaction of the atomic ensemble with the cavity microwave field creates added frequency shifts called the cavity pulling, microwave power shift and the propagation shift.

The cavity pulling is well known and is common to all masers. In the case of the CPT maser, which is a hybrid between an oscillating maser and a passive maser, the shift is function of the importance of the microwave power broadening of the resonance line and is given by (42). It creates a stringent demand on the tuning of the cavity, which should be stabilized to within the desired requirements. For a cavity Q_L of 10 000, a line Q_a of 5×10^7, the cavity must be stable to within 3 to 4 Hz to obtain a fractional frequency stability of $\sim 10^{-13}$.

The microwave power shift originates from the fact that upon microwave emission the populations of the ground levels are no longer equal. This creates an asymmetry in the system and an effect similar to the linear light shift mentioned above is introduced as shown in Fig. 12

An important effect predicted by the analysis is the introduction of a frequency shift associated with the phase of the sidebands radiation. The shift has been called a propagation shift and becomes rather important in the case of high densities (fractional shift = $\sim 10^{-9}$). This shift has been observed experimentally and is of the order of magnitude of that predicted [25].

VI CONCLUSION

In this paper we have reviewed our theoretical understanding of the coherent population trapping phenomenon as applied to the implementation of frequency standards. The review was made for both the passive and the maser approach.

- In particular we found that our understanding, using the EIT approach and the presence of optical pumping to trapping levels, is sufficient to explain most of the experimental observations made up to now.
- Both approaches are affected by common shifts particular to the CPT phenomenon such as a light shift. This light shift has various origins. In the passive approach the light shift caused by the difference in sidebands amplitude creates a distortion of the resonance line without affecting the resonance frequency, while in the maser it is a pure shift without distortion. There is also in both approaches a light shift created by the presence of off resonance sidebands. This shift consists of a quadratic light shift that is small and may be neglected, and a power light shift that can be reduced to a small value by using an appropriate modulation index, of about 2.4.
- The maser approach is affected by other shifts, such as microwave shift, propagation shift, and cavity pulling, that do not exist in the passive approach. However, these shifts may be well controlled and do not appear to create an impediment to the realization of frequency standards with attractive characteristics.

We conclude that the CPT phenomenon has opened avenues in the realization of two types of frequency standards that offer promises regarding simplicity of construction, small size and moderate frequency stability

REFERENCES.

[1] G. Alzetta., A. Gozzini, M. Moi and G. Orriols, “An experimental method for the observation of R.F. transitions and laser beat resonances in oriented Na vapour”, *Nuovo Cimento* B36, pp 5-20, 1976.

[2] N. Cyr, M. Têtu, and M. Breton, “All-optical microwave frequency standard: A proposal”, *IEEE Trans. Instrum. Meas*. IM42, pp. 640-649, 1993.

[3] J. Vanier, A. Godone and F. Levi, "Coherent population trapping in cesium: dark lines and coherent microwave emission", *Phys. Rev.* A58, pp. 2345-2358, 1998.

[4] A. Godone, F. Levi and J. Vanier, "Coherent microwave emission in cesium under coherent population trapping", *Phys. Rev.* A59, pp. R12-R15, 1999.

[5] J. Vanier and C. Audoin, "The Quantum Physics of Atomic Frequency Standards", Adam Hilger, Bristol, UK, 1989.

[6] G. Orriols, “Nonabsorption resonances by nonlinear coherent effects in a three-level system”, *Nuovo Cimento,* 53, pp. 1-24 1979.

[7] S.E. Harris, “Electromagnetically Induced Transparency”, *Phys. Today,* 50, pp. 36-42, 1997. A. Kasapi, M. Jain, G. Y. Yin, and S. E. Harris, “Electromagnetically Induced Transparency: propagation dynamics”, Phys. Rev. Letters 74, 2447-2450, 1995. See also: M. O. Scully and M. S. Zubairy, “Quantum Optics”, Cambridge University Press, Cambridge, UK, 1999.

[8] A. Godone, F. Levi, S. Micalizio and J. Vanier, “Dark line in optically thick vapors: inversion phenomena and line width narrowing”, *Eur. Phys. J*. D 18, pp. 5-13, 2002.

[9] F. Renzoni, A. Lindner and E. Arimondo, "Coherent population trapping in open systems: A coupled/noncoupled-state analysis", P*hys. Rev.* A 60, pp. 450-455, 1999. E. Arimondo, Coherent population trapping in laser spectroscopy, Progress in optics, E. Wolf, editor, pp. 257-354, 1996.

[10] Y. Sortais, “Construction d’une fontaine double à atomes froids de ^{87}Rb et ^{133}Cs; étude des effets dépendant du nombre d’atomes dans une fontaine". Thèse de doctorat, Université de Paris VI, Paris, France, 2001.

[11] Y. Sortais, et al., " Cold atoms clocks", *Physica Scripta*, T95, pp.50-57, 2001.

[12] D. J. Berkeland, J. D. Miller, J.C. Bergquist, W. N. Itano, and D. J. Wineland, "Laser cooled –atomic frequency standards", *Phys. Rev. Letters,* 80, pp. 2089-2092, 1998.

[13] C.D. Wallace, T.P. Dinneen, K-Y. N. Tan, T.T. Grove, P.L. Gould, " Isotopic difference in trap loss collisions of laser cooled Rb atoms", *Phys. Rev. Letters* 69, 897, 1992.

[14] R.H. Dicke, “The effect of collisions upon the Doppler width of spectral lines” *Phys. Rev. Letters* 18**,** 472-473, 1953.

[15] J. Vanier, M. Levine, D. Janssen and M. Delaney, “Coherent population trapping and intensity optical pumping: On their use in atomic frequency standards”, *Proc. of the 6th Symp on Freq. Stands. and Metrology*, pp. 155-166, 2001, St Andrews, Scotland, P. Gill, editor, World Scientific, London.

[16] J. Vanier, " Coherent population trapping for the realization of a small, stable, atomic Clock*", Proc. of the IEEE Int. Freq, Cont. Symp*. May 29-31, 2002, in press.

[17] J. E. Kitching, H.G. Robinson, and L. Hollberg, "Compact microwave frequency reference based on coherent population trapping", *Proc. of the 6th Symp on Freq. Stands. and Metrology*, pp. 167-174, 2001, St Andrews, Scotland, P. Gill, editor, World Scientific, London; J. Kitching, S. Knappe, and L. Hollberg, *"*Performance of small-scale frequency references", *Proc. of the IEEE Int. Freq, Cont. Symp*. May 29-31, 2002, in press. M. Merimaa, T. Lindvall, E. Tittonen, and E. Ikonen, “All optical atomic clock based on coherent population trapping in 85Rb”, JOSA B 20, 273-279, 2003.

[18] J. Vanier, "Relaxation in rubidium-87 and the rubidium maser", *Phys. Rev*. 168, pp. 129-149, 1968.

[19] J. Vanier and L.G. Bernier, "On the signal-to noise ratio and short-term stability of passive rubidium frequency

standards", *IEEE Trans. Instrum. & Meas.* IM-30, pp. 277-282, 1981.
[20] J. Vanier, M. Levine, D. Janssen and M. Delaney, " The coherent population trapping passive frequency standard", *IEEE Trans. Instrum. & Meas.* IM-52, 2003, in press.
[21] N. Sagna, C. Mandache, P. Thomann, "Noise measurement in single-mode GaAlAs diode lasers". *Proc. of the 6th Euro. Forum on Time and Frequency*, pp. 521-525, 1992.
[22] J.C. Camparo and W.F. Buell, "Laser PM to AM Conversion in Atomic Vapors and Short Term Clock Stability", *Proc. of the IEEE Int. Freq. Cont. Symp*. pp. 253-258, 1997; J.G. Coffer , M. Anderson, and J.C. Camparo, "Collisional dephasing and the reduction of laser phase-noise to amplitude–noise conversion in a resonant atomic vapor", *Phys. Rev*. 65, pp.033807-1-9, 2002. J. Kitching, H. G. Robinson, L. Hollberg, S. Knappe, R. Wynands, "Optical pumping noise in laser-pumped, all optical microwave frequency references" JOSA B 18, 1676-1683, 2001.
[23] A Godone, F Levi, S, Micalizio, "Coherent Population Trapping Maser", *C.L.U.T.,* editor, Torino Italy, 2002.
[24] J. Vanier, M. Levine, D. Janssen and M. Delaney, "Contrast and line width of the coherent population trapping transmission hyperfine resonance line in ^{87}Rb: Effect of optical pumping", *Phys Rev. A* in press.
[25] A. Godone, F. Levi, and S. Micalizio, "Propagation and density effects in the coherent-population trapping maser", *Phys. Rev*. A 65, pp. 033802-1-13, 2002.
[26] S. Knappe, J. Kitching, L. Hollberg, and R. Wynands, "Temperature dependence of coherent population trapping resonances", *Appl. Phys.* B 74, pp. 217-222, 2002.
[27] J. Vanier, "Atomic Frequency Standards: Basic and impact on metrology", in *Recent advances in metrology and fundamental constants*, pp. 397-452, T.J. Quinn, S Leschiutta, and P. Tavella, editors, IOS Press, 2000
[28] A. Godone, F. Levi, S. Micalizio and J. Vanier, "Theory of the coherent population trapping maser: A strong field approach", *Phys. Rev.* A62, pp. 053402-1-11, 2000.
[29] L. L. Lewis and M.Feldman, "Optical pumping by lasers in atomic frequency standards", *Proc. of the 35th Ann. Symp. on Frequency Control*, (Washington DC: Electronic Industries Association), p. 612, 1981.
[30] G. Mileti, J.Q. Deng, F.L. Walls, D.A. Jennings, R.E. Drullinger, "Laser pumped rubidium frequency standards: New analysis and progress". *IEEE J Quant. Electron.* 34, pp. 233-237, 1998. G. Mileti, J.Q. Deng, F.L. Walls, J.P. Lowe, R.E. Drullinger, "Recent progress in laser-pumped rubidium gas-cell frequency standards", *Proc. IEEE Int. Freq. Cont. Symp*., pp. 1066-1072, 1996.
[31] J. Vanier, R. Kunski, N. Cyr, and M. Têtu, "On hyperfine frequency shifts caused by buffer gases: Application to the optically pumped passive rubidium frequency standard", *J. Appl. Phys*. 53, pp. 5387-5389, 1982.
[32] F. Levi, A. Godone, J. Vanier, S. Micalizio and G. Modugno, "Line shape of dark line and maser emission profile in CPT", *Eur. Phys. J.* D12, pp. 53-59, 2000.
[33] F. Levi, A. Godone and J. Vanier, "The Light Shift Effect in the Coherent Population trapping Cesium Maser", *IEEE Trans. Ultras. Ferroel. and Freq. Cont*. 47, pp. 466-471, 2000.
[34] M. Zhu and L. Cutler, "Theoretical and Experimental Study of Light Shift in CPT-Based Rb vapor Cell frequency Standard", Proc of the *Precise Time and Time Interval (PTTI) Systems and Applications Meeting,* Reston, Virginia, USA (2000).
[35] J. P. Barrat et C. Cohen-Tannoudji, "Étude du pompage optique dans le formalisme de la matrice densité", *Le Journal de Phys. et le Radium* 22, pp. 329-336, 1961.

Appendix

Optical absorption of polarized laser radiation

This Appendix concerns optical absorption spectra of the cell used in the CPT passive approach experiments described in this paper. The level structure of the lower manifold of ^{87}Rb pertinent to the present discussion is shown in Fig. A1.

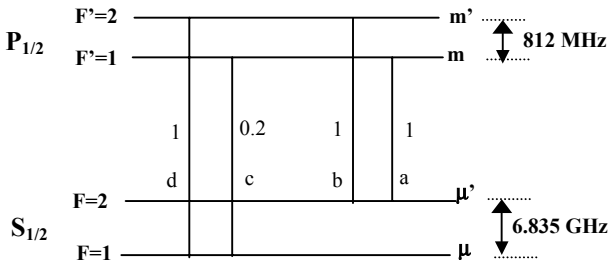

Figure A1. Lower levels $P_{1/2}$ and $S_{1/2}$ of the ^{87}Rb atom. The numbers in circles are transition probabilities summed over the Zeeman sublevels of each manifold.

The absorption spectra under various conditions are shown in Fig. A2. The spectra are obtained for two light intensities and two polarizations, linear polarization propagating in the direction of the magnetic field, called σ, and circular polarization, σ^+ (or σ^-). As is clearly observed in that figure there is a drastic change in behavior in passing from linear polarization to circular polarization. Absorption through transition "a" is considerably reduced under circular polarization. Transition probability between the various Zeeman sublevels cannot explain alone this behavior. In fact a summation over all these levels considering appropriate transitions give equal transition probabilities whatever the polarization. The effect can only be explained through a detailed examination of the dynamics of the transitions causing optical pumping. This is shown in Fig. A3 for the case of σ^+ polarization. As is observed, for transition "a" levels F=2, m_F = 1 and 2 are not connected by

the radiation. For transition "b", only level F=1, m_F=2 is not connected. Atoms excited to the P state decay to all levels equally due to collisions with the buffer gas and are trapped in these levels. This effect is essentially an optical pumping process [35]. Decay from the excited state takes place at rate Γ^* (~10^9 s^{-1}), while equilibrium in the ground state is reestablished through relaxation at rate γ_1 (~10^3 s^{-1}). There are thus a large number of atoms trapped in these levels and they no longer contribute to absorption.

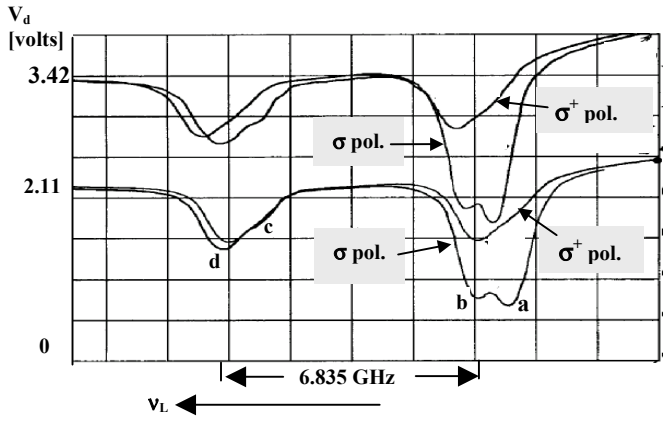

Figure A2. Absorption spectrum of a ^{87}Rb cell under linear polarization (σ) and circular polarization (σ^+). The laser is not modulated. The absorption lines are identified by "a", "b", "c", and "d" corresponding to the transitions shown in Fig. A1. The absorption spectrum is shown for two light intensities of 21 μwatts (2.11 volts) and 34 μwatts (3.42 volts) incident on the cell [M. Levine and D. Janssen, private communication].

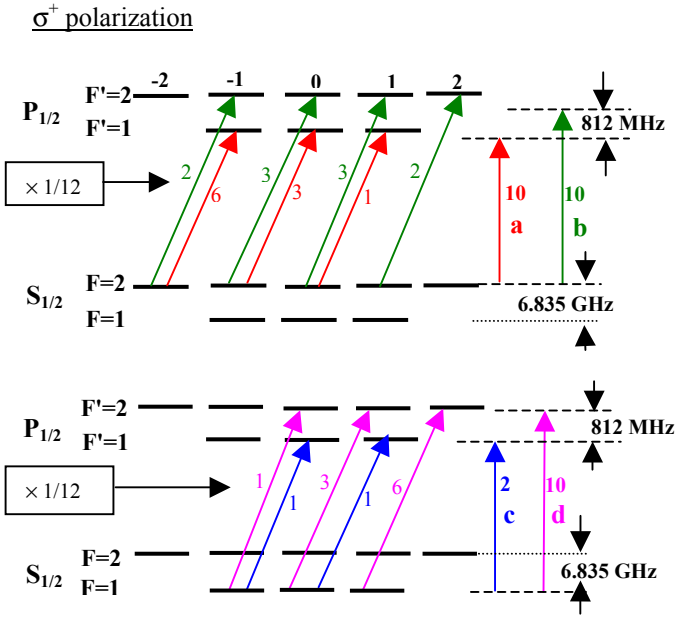

Figure A3. Manifold of ^{87}Rb lower energy levels used to illustrate the characteristics of optical absorption. The numbers attached to the arrow are transition probabilities.

The situation for transitions "c" and "d" originating from level F=1 is different, as is seen in Fig A3. Only level F=1, m_F=1 can act as a trap for transition "c". However, in all cases the other hyperfine level not involved in the transition can also act as a trap. The only difference between the two cases is related to the number of trapping levels involved. In the case of σ polarization the situation is radically different. A similar representation as that shown in Fig. A3 shows that transitions are possible from all Zeeman sublevels and there are no trapping levels as in the previous case. Optical pumping is possible only to the other hyperfine level not involved in the transition.

An analysis can be made of this effect using the tools developed in the present paper. Since there is only one radiation field present there is no coherence introduced in the ground state. Solving (28) through numerical integration, we can calculate readily the intensity of the transmitted radiation (square of the amplitude of the optical Rabi frequency) at the exit of the cell. The required expression of the optical coherence is calculated from rate equations similar to the set 16-21. In the calculation we assume the appropriate number of trap levels as determined from Fig. A3 for σ^+ polarization, and from a similar one for σ polarization. We use tabulated values of transition probabilities. This is done for two intensities approximating the experimental situation shown in Fig. A2. The result of this exercise is shown in Fig. A.4.

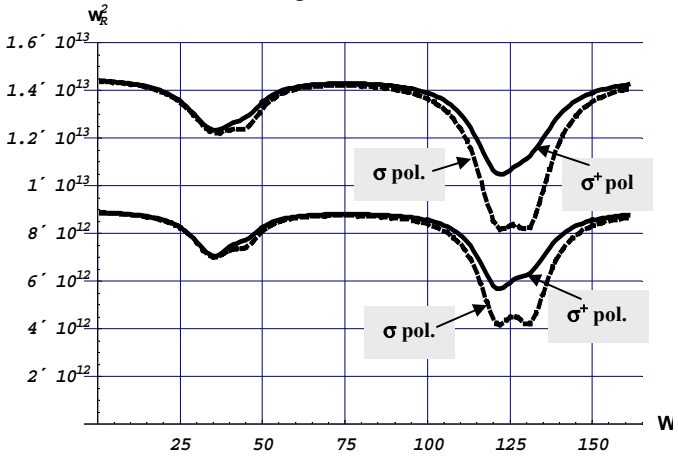

Figure A4. Calculated absorption spectrum (D1) by a cell containing ^{87}Rb and a buffer gas for two values of the intensity of a monochromatic laser radiation corresponding approximately to those used in the case of Fig. A2. The constants assumed in the calculation are α= 2.1 x10^{11} m^{-1} s^{-1} and Γ^*= 2 x 10^9 s^{-1}.

These results can be compared to the actual absorption spectrum of laser radiation shown in Fig A2. It appears that the model developed based on optical pumping explains rather well at least qualitatively the experimental observations. The net effect is a transfer of population from absorbing levels to other levels not coupled by the radiation, decreasing considerably the absorption and affecting the shape of the overlapping absorption lines. The present results validates to a certain extent the 4-level model that was used in the calculation outlined above on the CPT hyperfine resonance contrast.